Meteoritics & Planetary Science 38, Nr 10, 1507–1520 (2003)
Abstract available online at http://meteoritics.org

Spade: An H chondrite impact-melt breccia that experienced post-shock annealing

Alan E. RUBIN[1*] and Rhian H. JONES[2]

[1]Institute of Geophysics and Planetary Physics, University of California, Los Angeles, California 90095–1567, USA
[2]Institute of Meteoritics, Department of Earth and Planetary Sciences, University of New Mexico, Albuquerque, New Mexico 87131, USA
[*]Corresponding author. E-mail: aerubin@ucla.edu

(Received 26 January 2003; revision accepted 19 October 2003)

Abstract–The low modal abundances of relict chondrules (1.8 vol%) and of coarse (i.e., ≥200 μm-size) isolated mafic silicate grains (1.8 vol%) in Spade relative to mean H6 chondrites (11.4 and 9.8 vol%, respectively) show Spade to be a rock that has experienced a significant degree of melting. Various petrographic features (e.g., chromite-plagioclase assemblages, chromite veinlets, silicate darkening) indicate that melting was caused by shock. Plagioclase was melted during the shock event and flowed so that it partially to completely surrounded nearby mafic silicate grains. During crystallization, plagioclase developed igneous zoning. Low-Ca pyroxene that crystallized from the melt (or equilibrated with the melt at high temperatures) acquired relatively high amounts of CaO. Metallic Fe-Ni cooled rapidly below the Fe-Ni solvus and transformed into martensite. Subsequent reheating of the rock caused transformation of martensite into abundant duplex plessite.

Ambiguities exist in the shock stage assignment of Spade. The extensive silicate darkening, the occurrence of chromite-plagioclase assemblages, and the impact-melted characteristics of Spade are consistent with shock stage S6. Low shock (stage S2) is indicated by the undulose extinction and lack of planar fractures in olivine. This suggests that Spade reached a maximum prior shock level equivalent to stage S6 and then experienced post-shock annealing (probably to stage S1). These events were followed by a less intense impact that produced the undulose extinction in the olivine, characteristic of shock stage S2. Annealing could have occurred if Spade were emplaced near impact melts beneath the crater floor or deposited in close proximity to hot debris within an ejecta blanket. Spade firmly establishes the case for post-shock annealing. This may have been a common process on OC asteroids.

INTRODUCTION

Many ordinary chondrites (OC) exhibit evidence of impact melting. Many contain impact-melt-rock clasts (e.g., Plainview, Tysnes Island, Johnson City) that formed from small-scale impacts into the host (Fodor and Keil 1976; Wilkening 1978; Rubin et al. 1983). Some OC are impact-melt breccias (e.g., Rose City, Cat Mountain, Chico) that contain large impact-melted regions adjacent to relict chondritic regions (Mason and Wiik 1966; Kring et al. 1996; Bogard et al. 1995). A few OC are impact-melt rocks (e.g., PAT 91501, Y-74160, Y-790964, Ramsdorf) that have been extensively or completely melted (Mittlefehldt and Lindstrom 2001; Takeda et al. 1984; Yamaguchi et al. 1998, 1999); they contain little relict chondritic material.

Some OC have been shocked and annealed (e.g., Rubin 2002, Forthcoming). Annealing may have been caused by burial of these samples in proximity to impact melts beneath the floor of an impact crater or near hot debris in an ejecta blanket. The identification of an OC impact-melt breccia that was shocked and annealed would confirm the reality of complex thermal processing on OC asteroids. Different components of the meteorite could record different episodes of the rock's thermal and shock history.

Spade appears to be an annealed impact-melt breccia. The meteorite was found as a single 8.9 kg stone at a location 8.5 km north and 1.6 km east of the town of Spade in Lamb County, Texas.

ANALYTICAL PROCEDURES

Polished thin section UNM 1099 (~185 mm^2) of Spade was studied microscopically in transmitted and reflected light. Grain sizes were measured with a petrographic microscope using a calibrated reticle. Modal abundances were determined microscopically using an automated point counter. Polished slab C359.1 (~2500 mm^2) from the collection of the Institute of Meteoritics at the University of New Mexico was examined

microscopically. The thin section and slab were etched with a dilute solution of nitric acid to reveal metallographic details.

Quantitative analyses of olivine, plagioclase, chromite, metal, and sulfide were performed using the JEOL 733 Superprobe electron microprobe at UNM, with operating conditions of 15 kV and a beam current of 20 nA. Silicate standards were used for silicate minerals, and a combination of metal and sulfide standards was used for metal and sulfide mineral analyses. Low-Ca pyroxene and Ca pyroxene were analyzed with the JEOL JXA-8200 electron microprobe at UCLA, using natural and synthetic standards, an accelerating voltage of 15 keV, a 15 nA sample current, 20 sec counting times, and ZAF corrections.

RESULTS

Weathering Grade

Thin section and slab examination indicate that ~60% of the silicate grains exhibit significant brown staining. Many mafic silicate grains are traversed and surrounded by 0.1 μm-thick veins of limonite (α-FeO[OH]). The majority of metallic Fe-Ni grains in the interior appear unaltered; they lack limonite rims and are consistent with weathering stage W1 (Wlotzka 1993). However, within 3–4 mm of the meteorite surface, brown staining is much more extensive and most metal and sulfide grains have been largely or completely altered. Numerous subparallel 10–100 μm-thick veins and associated veinlets of limonite occur in these extensively weathered regions, consistent with weathering stage W5.

Chondrite Group

Modal analysis (Table 1) indicates that Spade contains 18.2 wt% metallic Fe-Ni; this is half way between the normative mineralogical value of H chondrites (18.6 wt%; Table 4.1 in Dodd 1981) and the mean of H chondrite falls analyzed by wet chemistry (17.8 wt%; Jarosewich 1990). This is much higher than the values for L and LL chondrite falls (8.3 and 3.6 wt%, respectively; Jarosewich 1990).

Mineral compositions also indicate that Spade is an H-group chondrite. The mean olivine and low-Ca pyroxene compositions in Spade ($Fa_{19.0}$ and $Fs_{16.0}$, respectively; Table 2) are within the H4–6 chondrite ranges ($Fa_{16–20}$, $Fs_{14.5–18}$; Brearley and Jones 1998). The mean plagioclase composition (n = 24) of $Ab_{79.9}Or_{4.8}$ (Table 2) is closest to the mean of H chondrite plagioclase ($Ab_{81.9}Or_{5.8}$; Van Schmus and Ribbe 1968) and appreciably less sodic than the mean compositions of plagioclase in L and LL chondrites (i.e., $Ab_{84.2}Or_{5.6}$ and $Ab_{85.9}Or_{3.6}$, respectively). The mean kamacite Co content of Spade (0.46 ± 0.03 wt%; Table 3) is within the H chondrite range (0.44–0.51 wt% Co; Rubin 1990) and the kamacite Ni content (6.9 wt%; Table 3) is identical to the mean value in H4–6 chondrites (Rubin 1990).

Texture and Mineral Chemistry

The Spade whole-rock does not appear to be brecciated; no clasts are visible in the slab. The rock is rich in metallic Fe-Ni and contains metal veins. One curvilinear metal vein is

Table 1. Modal abundances of major phases in Spade.[a]

	Vol%	Wt%	Mean H (wt%)[b]
Silicate	84.5	73.5	74.7
Troilite	5.4	6.6	5.3
Metallic Fe-Ni	8.7	18.2	18.6
Chromite	0.6	0.7	0.6
Limonite	0.8	0.9	–
Total	100.0	99.9	100.0
Nr of points	2190	2190	–
Area (mm^2)	200	200	–

[a]Vol% percent was converted into wt% using the following specific gravities: silicate, 3.3; troilite, 4.67; metallic Fe-Ni, 7.95; chromite, 4.7; limonite, 4.28.

[b]Normative mineralogy from Table 4.1 in Dodd (1981); total includes 0.6 wt% apatite and 0.2 wt% ilmenite.

Table 2. Compositions (wt%) of silicate and oxide phases in Spade.[a]

	Olivine	Low-Ca pyx	Ca pyx	Plagioclase	Chromite
Nr of grains	9	7	10	24	10
SiO_2	39.1 ± 0.4	55.7 ± 0.4	53.6 ± 0.3	64.8 ± 2.0	<0.04
TiO_2	<0.04	0.27 ± 0.05	0.41 ± 0.06	–	1.9 ± 0.2
Al_2O_3	<0.04	0.36 ± 0.09	0.99 ± 0.10	22.6 ± 1.5	3.5 ± 0.7
Cr_2O_3	0.04 ± 0.01	0.57 ± 0.11	1.5 ± 0.12	n.d.	60.6 ± 0.7
V_2O_3	n.d.	n.d.	n.d.	n.d.	0.67 ± 0.07
FeO	17.9 ± 0.3	10.7 ± 0.1	5.1 ± 0.2	0.55 ± 0.14	27.4 ± 1.1
MnO	0.52 ± 0.02	0.52 ± 0.05	0.29 ± 0.03	n.d.	0.91 ± 0.08
MgO	42.9 ± 0.2	30.2 ± 0.4	17.8 ± 0.2	<0.04	4.8 ± 0.7
CaO	<0.04	1.8 ± 0.2	19.3 ± 0.2	3.3 ± 1.7	n.d.
Na_2O	<0.04	0.08 ± 0.03	0.73 ± 0.07	9.4 ± 0.7	n.d.
K_2O	n.d.	<0.02	<0.02	0.86 ± 0.48	n.d.
Total	100.5	100.2	99.8	101.5	99.8
End member	$Fa_{19.0 \pm 0.3}$	$Fs_{16.0 \pm 0.1}Wo_{3.5 \pm 0.4}$	$Fs_{8.4 \pm 0.3}Wo_{40.2 \pm 0.5}$	$Ab_{79.9 \pm 5.7}Or_{4.8 \pm 2.7}$	

[a]n.d. = not determined.

Table 3. Compositions (wt%) of opaque phases in Spade.[a]

	Kamacite	Plessite	Troilite	Pent
Nr of grains	28	9	18	1
Fe	92.8 ± 1.0	88.0 ± 3.5	63.8 ± 0.3	56.4
Ni	6.9 ± 0.5	11.6 ± 3.3	<0.04	8.7
Co	0.46 ± 0.03	0.34 ± 0.08	<0.04	<0.04
S	n.d.	n.d.	35.7 ± 0.7	34.2
Total	100.2	99.9	99.5	99.3

[a]n.d. = not determined; pent = pentlandite.

~4 cm long and ~0.8 mm thick. Thin section observations show that Spade has a compact, recrystallized texture composed of interlocking silicate (olivine, low-Ca pyroxene, Ca pyroxene, plagioclase), metallic Fe-Ni (kamacite, taenite, plessite), sulfide (troilite, pentlandite), and chromite grains.

Although many of the olivine and pyroxene grains occur in relatively coarse clusters, throughout the meteorite, interstitial fine-grained regions exist (Fig. 1), consisting of (in vol%): ~70% olivine, 15% plagioclase, 10% low-Ca pyroxene, and 5% metallic Fe-Ni and sulfide. Grain sizes in these areas are typically 10–25 μm. In some cases, the olivine grains are adjacent to one another and are tightly packed; in others, they are separated by 10–50 μm-size patches of plagioclase. These regions seem similar to impact-melted regions in the Ramsdorf impact-melt rock (e.g., Fig. 2c in Yamaguchi et al. 1999).

Modal analysis (2868 points) of the thin section indicates that Spade contains 1.8 vol% relict barred olivine (BO) and porphyritic olivine-pyroxene (POP) chondrules. The relict chondrules are highly recrystallized and range in size from 300 to 1000 μm. They exhibit extensive silicate darkening caused by the dispersion in the silicate phenocrysts of 0.2–4 μm-size opaque blebs, mainly troilite. Some relict chondrules are adjacent to small fine-grained regions and appear to be overgrown by numerous 25 μm-size olivine grains that crystallized from the melt. The modal abundance of relict chondrules in Spade is much lower than those in typical H5 and H6 chondrites (i.e., 22.1 ± 6.7 vol% and 11.4 ± 3.6 vol%, respectively; Table 2 in Rubin et al. 2001).

Spade also contains 1.8 vol% coarse (≥200 μm-size) mafic silicate grains, most of which exhibit extensive silicate darkening (Figs. 2a, 2b, and 3). The modal abundance of these grains is much lower than those in typical H5 and H6 chondrites (i.e., 9.0 ± 2.1 vol% and 9.8 ± 2.1 vol%, respectively; Table 2 in Rubin et al. 2001).

Plagioclase patches are typically 100–200 μm in size and are irregular in shape. Many plagioclase grains in the thin section and across the 8.5 cm-long slab are shaped like pincers and wrap around (i.e., partially to completely enclose) adjacent 5–20 μm-size olivine grains (Fig. 4). Some plagioclase grains have 2 or 3 sets of pincer-shaped appendages. Most plagioclase

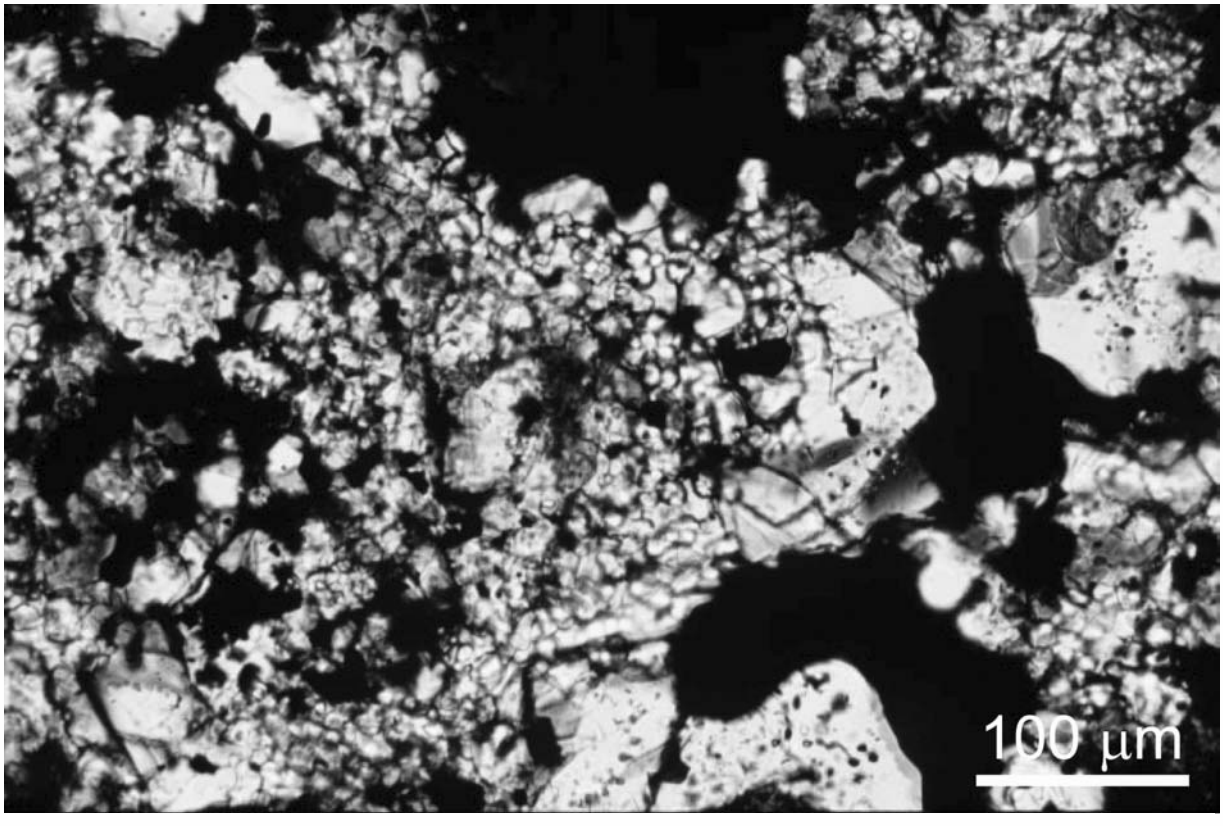

Fig. 1. Fine-grained region consisting mainly of 10–25 μm-size grains of olivine, plagioclase, and low-Ca pyroxene. Metal and troilite grains (right of center) appear black. Transmitted light.

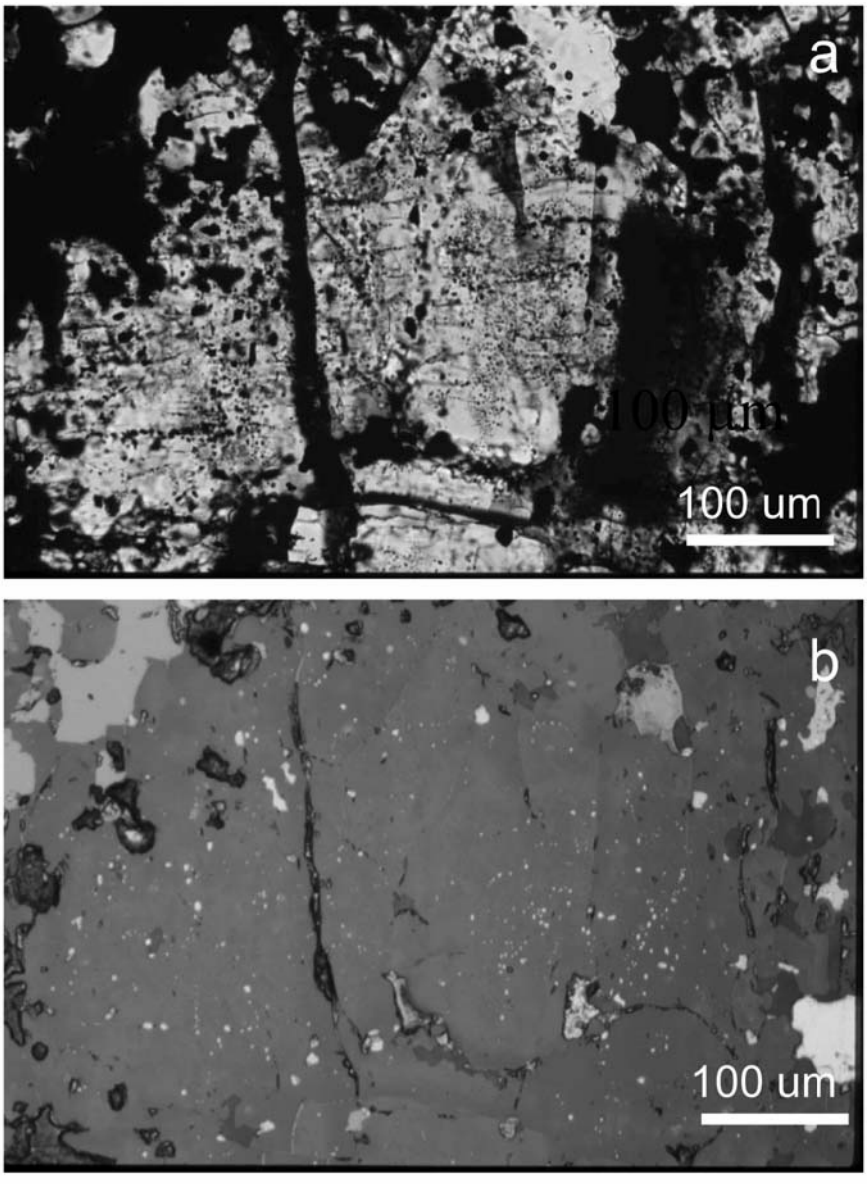

Fig. 2. Coarse olivine grain containing numerous small opaque blebs (mainly troilite with minor metallic Fe-Ni); most of the small opaque blebs are within curvilinear trails that transect the olivine grain: a) transmitted light view showing significant silicate darkening; b) reflected light view showing some of the small opaque blebs (white). The abundance of blebs appears lower in reflected light because only those blebs that are at the surface of the 30 µm-thick thin section are visible.

patches are adjacent to (or partly surround) metallic Fe-Ni and/or troilite grains; a few plagioclase patches are completely surrounded by mafic silicate grains.

Olivine and low-Ca pyroxene are relatively homogeneous in composition ($Fa_{19.0 \pm 0.3}$ and $Fs_{16.0 \pm 0.1}$, respectively; Table 2), indicative of equilibrium and typical of H4–6 chondrites. However, the CaO content of the low-Ca pyroxene (1.8 wt%; 3.5 ± 0.4 mol% Wo) is much higher than that in typical H chondrites (e.g., Wo <2.4 mol%; Scott et al. 1986). The apparent absence of polysynthetically twinned low-Ca pyroxene suggests that all of the low-Ca pyroxene in Spade is orthorhombic.

Ca pyroxene is also relatively homogeneous in composition (8.4 ± 0.3 mol% Fs). Its CaO content of 19.3 wt% (40.2 ± 0.5 mol% Wo) puts it in the compositional range of endiopside.

Plagioclase compositions are somewhat variable (Table 2). The An component ($An_{15.3 \pm 7.9}$) ranges from 4.6 to 28.8 mol%; the Or component ($Or_{4.8 \pm 2.7}$) ranges from 1.4 to 12.0 mol%. Individual plagioclase grains in Spade are compositionally zoned; they possess relatively calcic, low-Na_2O cores ($Ab_{68–71}Or_{2.2–2.5}$) and relatively sodic and potassic rims ($Ab_{83–85}Or_{6–8}$).

Chromite occurs as 25–200 µm-size grains adjacent to

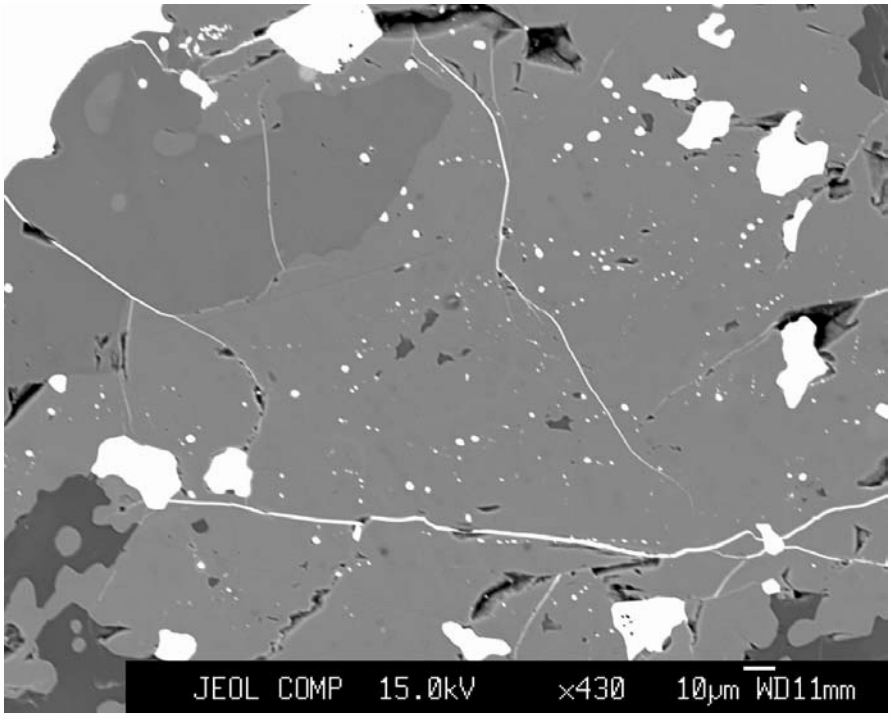

Fig. 3. Numerous small blebs of metallic Fe-Ni (white) inside mafic silicate grains (dark gray) causing significant silicate darkening in Spade. Back scattered electron image. The scale bar is 10 μm long.

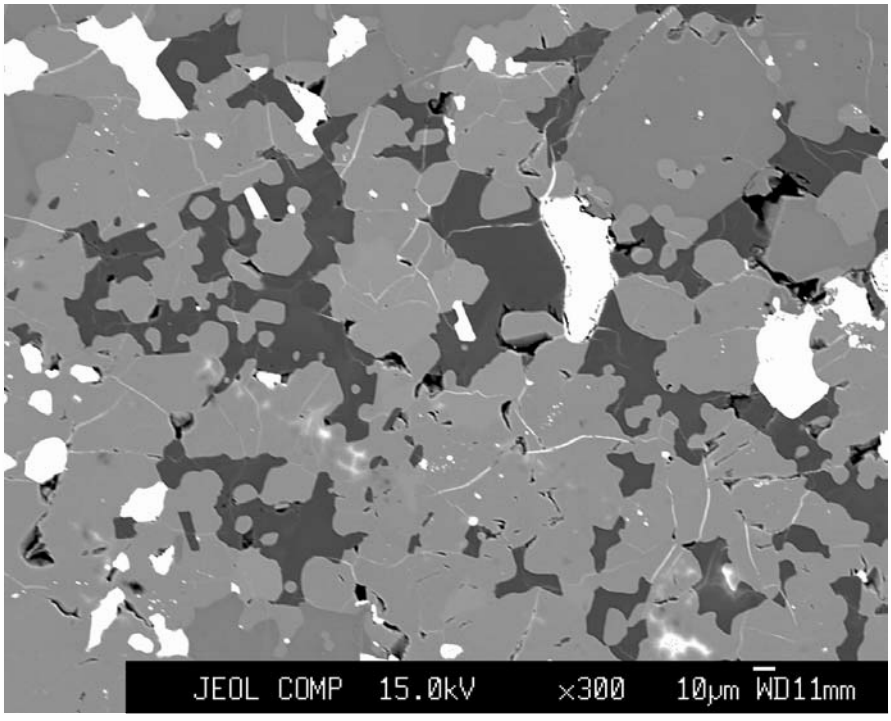

Fig. 4. Pincer-shaped plagioclase patches (dark gray) partially to completely surrounding small mafic silicate grains (medium gray). The plagioclase has apparently melted and flowed following impact heating. Many of the plagioclase patches are adjacent to metallic Fe-Ni (white). Back scattered electron image. The scale bar is 10 μm long.

metallic Fe-Ni and troilite, as isolated grains completely surrounded by mafic silicate, and in chromite veinlets and chromite-plagioclase assemblages (described below). The mean composition of chromite outside the veinlets and chromite-plagioclase assemblages in Spade is appreciably lower in Al_2O_3 (3.5 wt%) and FeO (27.4 wt%) and higher in MgO (4.8 wt%) than that of equilibrated H chondrites (5.6–7.3 wt% Al_2O_3; 29.4–32.0 wt% FeO; 2.0–3.2 wt% MgO; Table 2 in Bunch et al. 1967; see also Fig. 191 of Brearley and Jones [1998]).

Metallography

Although the largest metallic Fe-Ni grains in Spade are quasi-equant and ~1.2 mm in maximum dimension, such grains are rare. The mean size of metal grains is 170 ± 95 μm (n = 108), comparable to, or slightly larger than, those in typical H5 and H6 chondrites (120 ± 150 μm; Table 2 of Rubin et al. 2001). Some metallic Fe-Ni grains consist exclusively of kamacite; many of these are adjacent to small patches of troilite. Most kamacite-troilite interfaces are curved, suggestive of an igneous origin (Scott 2003, personal communication). None of the metal grains in Spade contains schreibersite.

Some kamacite grains are partly surrounded by relatively coarse (~130–150 μm-size) grains of phosphate, either merrillite by itself or merrillite plus chlorapatite (Fig. 5). Some similarly sized grains of merrillite occur at the metal-silicate boundary in the Portales Valley impact-melt breccia (e.g., Ruzicka et al. 1999; Rubin et al. 2001).

Many grains of metallic Fe-Ni in the thin section and across the slab consist of kamacite surrounding rounded to oblong patches of duplex plessite (Figs. 6a and 6b); the plessite constitutes 10–80 vol% of these metallic Fe-Ni grains. (As defined by Buchwald [1975], e.g., Fig. 129, duplex plessite consists of intricate intergrowths of 0.5–2 μm-size kamacite and taenite particles.) The plessite regions in Spade metal are typically surrounded by a ~0.5–2 μm-thick rim of taenite. The duplex plessite consists of 1 × 5 μm- to 6 × 30 μm-size sparks and spindles of kamacite surrounded by irregularly shaped fine-grained plessite regions. A few metallic Fe-Ni grains are completely composed of duplex plessite.

Some kamacite grains enclose patches of net plessite consisting of 2–10 μm-diameter rounded kamacite blebs flanking 5 × 40 μm-size kamacite shafts; some kamacite sparks and spindles also occur in these grains. (As defined by Buchwald [1975], e.g., Fig. 124, net plessite consists of 1–10 μm-size islands of taenite within kamacite that contains numerous boundaries and subboundaries.) A few net plessite occurrences in Spade are coarser and contain quasi-equant 5–15 μm-size cells and shafts of kamacite (Fig. 6c). In some cases, a 3–4 μm-thick zone of very fine-grained plessite occurs between the net plessite and the 0.5 μm-thick taenite rim.

Electron microprobe analysis of plessite regions yields a mean Ni content of 11.6 ± 3.3 wt% (Table 3) and a range of 8.4–16.6 wt% Ni. This variability is due to electron beam

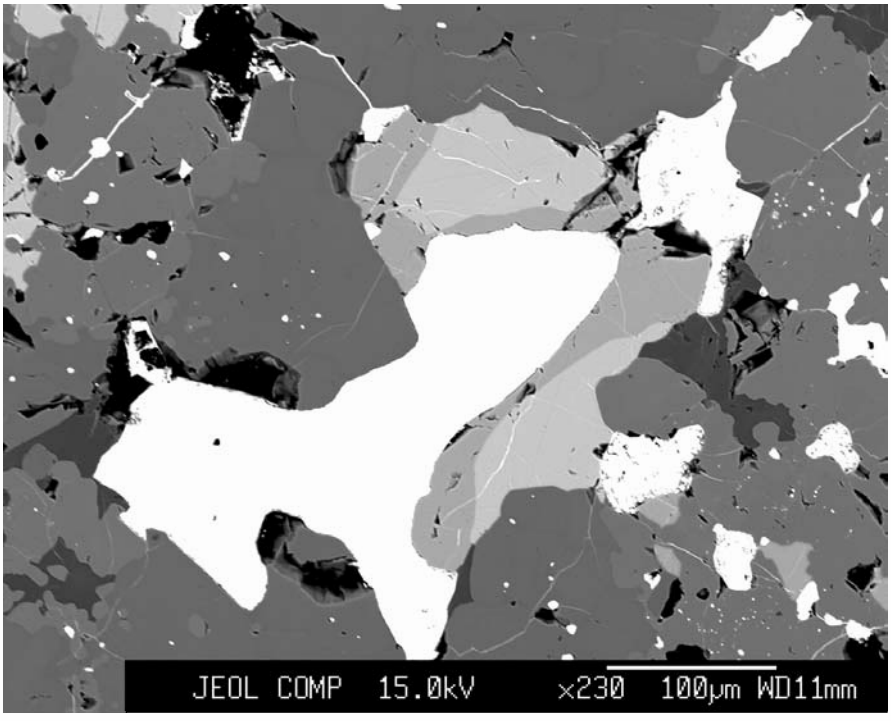

Fig. 5. Kamacite grain (white) rimmed by two phosphate phases. The innermost rim (medium gray) is merrillite; the outer rim (light gray) is chlorapatite. The entire assemblage is surrounded by silicate (dark gray to black). Back scattered electron image. The scale bar is 100 μm long.

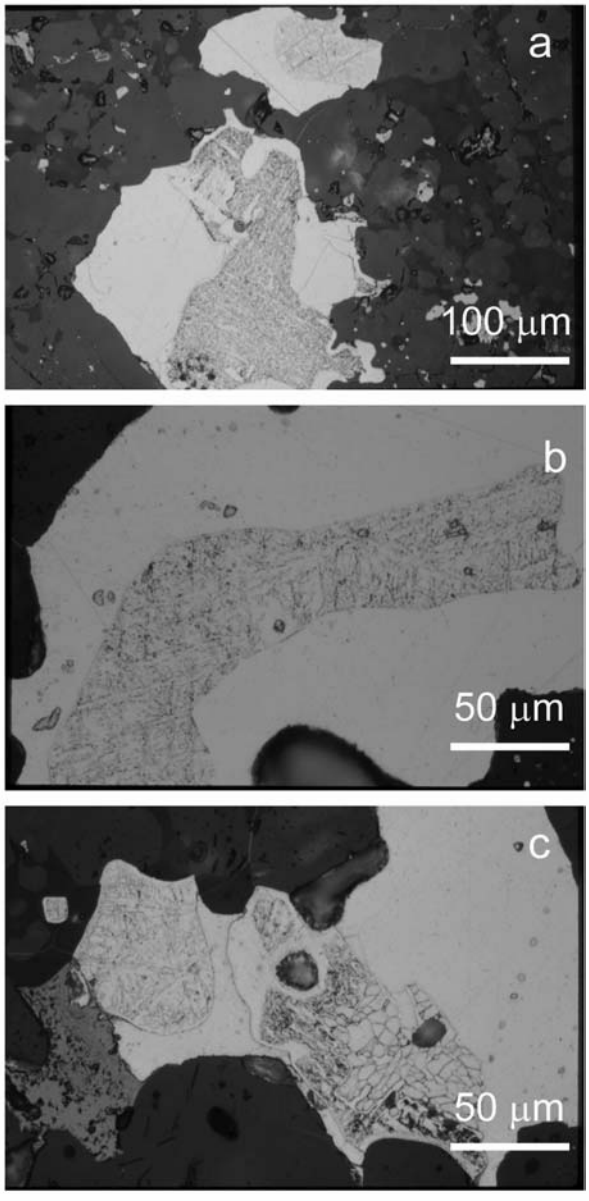

Fig. 6. Grains of metallic Fe-Ni consisting of kamacite (light gray to white) surrounding patches of plessite in nital-etched thin section: a) a large patch of duplex plessite (medium gray) consisting of small sparks and spindles of kamacite. The plessite constitutes ~50 vol% of the metal grain; b) a patch of duplex plessite containing small sparks and spindles of kamacite; this plessite patch constitutes ~20 vol% of the metal grain in which it occurs; c) two plessite patches within a kamacite grain. Duplex plessite occurs at left. The patch of net plessite on the right is composed of rounded kamacite blebs and elongated kamacite shafts. A thick taenite rim (white; center) occurs at the upper left side of the net plessite patch. All images are in reflected light.

overlap of small kamacite and taenite grains in different proportions. The analyzed spots with higher Ni contents contain a higher proportion of taenite and have lower Co contents than the lower-Ni spots (which contain a higher proportion of kamacite).

Sulfide

Troilite grains in Spade have a mean size of 75 ± 55 μm (n = 109), comparable to those in typical H5 (75 ± 70 μm) and H6 chondrites (80 ± 60 μm) (Table 2 in Rubin et al. 2001). Most troilite grains are adjacent to coarse grains of metallic Fe-Ni and form curved interfaces with the metal (Fig. 7).

Electron microprobe analysis indicates that the troilite grains are pure FeS (Table 3); Ni and Co are below the limits of detection (~0.04 wt%). One rare grain of pentlandite with 8.7 wt% Ni was analyzed (Table 3).

Shock Features

Shock Stage

Although most small olivine grains in fine-grained regions are unstrained and exhibit sharp optical extinction, many coarse olivine grains outside the fine-grained regions exhibit undulose extinction. This indicates that the Spade whole-rock is shock stage S2 (Stöffler et al. 1991). This low degree of shock stands in contrast to such shock features as extensive silicate darkening (Figs. 2 and 3) and the occurrence of chromite-plagioclase assemblages (see below).

Silicate Darkening

Spade exhibits extensive silicate darkening caused by randomly distributed 0.5–4 μm-size blebs of metallic Fe-Ni, troilite, and chromite inside mafic silicate grains. Also present in the silicate grains throughout the meteorite are 20–50 μm-long curvilinear trails of opaque grains. Most trails consist of 0.5–4 μm-size blebs of troilite, a few trails are composed of blebs of metallic Fe-Ni and troilite, and some trails consist of 0.2–0.5 μm-size blebs of chromite. A few of the chromite trails (e.g., Fig. 8) contain 0.7 × 2 μm-size chromite needles and chromite blebs.

Rapidly Solidified Troilite-Metal Intergrowths

Many of the troilite grains contain 2–15 vol% small (2–4 μm-size) blebs, cells, and irregularly shaped patches of metallic Fe-Ni (e.g., Fig. 7). They resemble the rapidly solidified troilite-metal mixtures that are present in many shocked OC (e.g., Scott 1982). Possibly, these mixtures represent late-stage shock and do not date from the event that caused wide-spread melting in Spade.

Chromite-Plagioclase Assemblages

Approximately 15 vol% of the chromite in Spade (thin section and slab) occurs in chromite-plagioclase assemblages (Fig. 9). Modal abundance determinations (2190 points) indicate that Spade contains 0.5 vol% of these assemblages. The assemblages range in size from ~50–620 μm and in chromite/plagioclase modal ratio from 0.05–0.33. The largest chromite-plagioclase assemblage observed in Spade is quasi-equant and ~620 μm in diameter. It consists of ~20 vol%

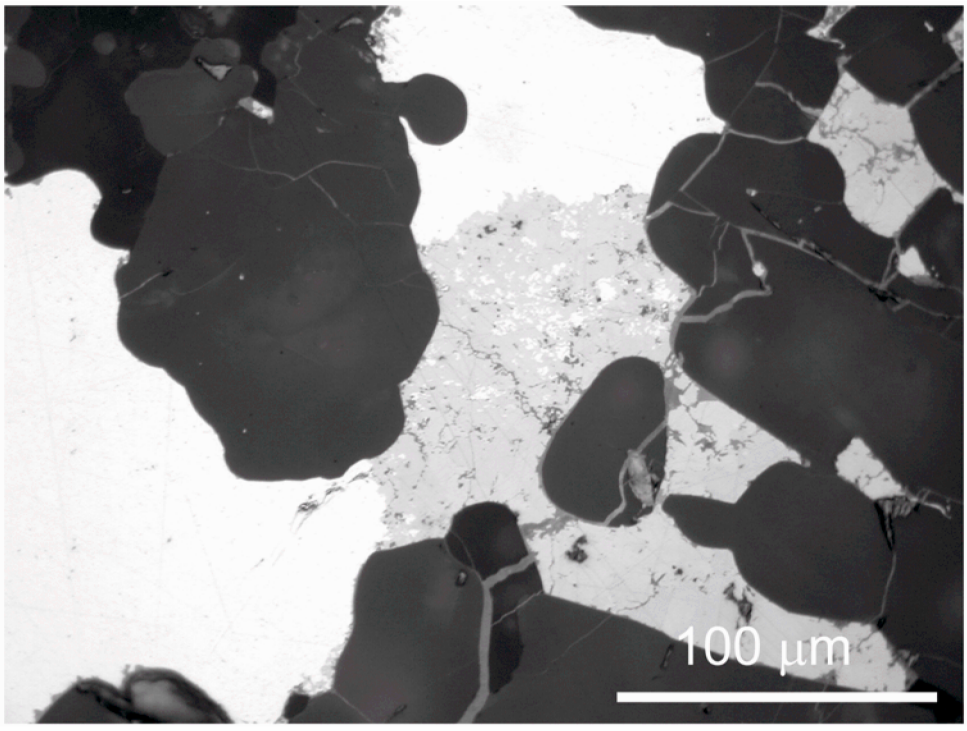

Fig. 7. Troilite grain (medium gray) flanked by coarse metallic Fe-Ni grains (white) and containing small irregularly shaped metal patches (white; center). Similar fine-grained metal-troilite intergrowths with high troilite/metal modal-abundance ratios occur throughout the meteorite. Reflected light.

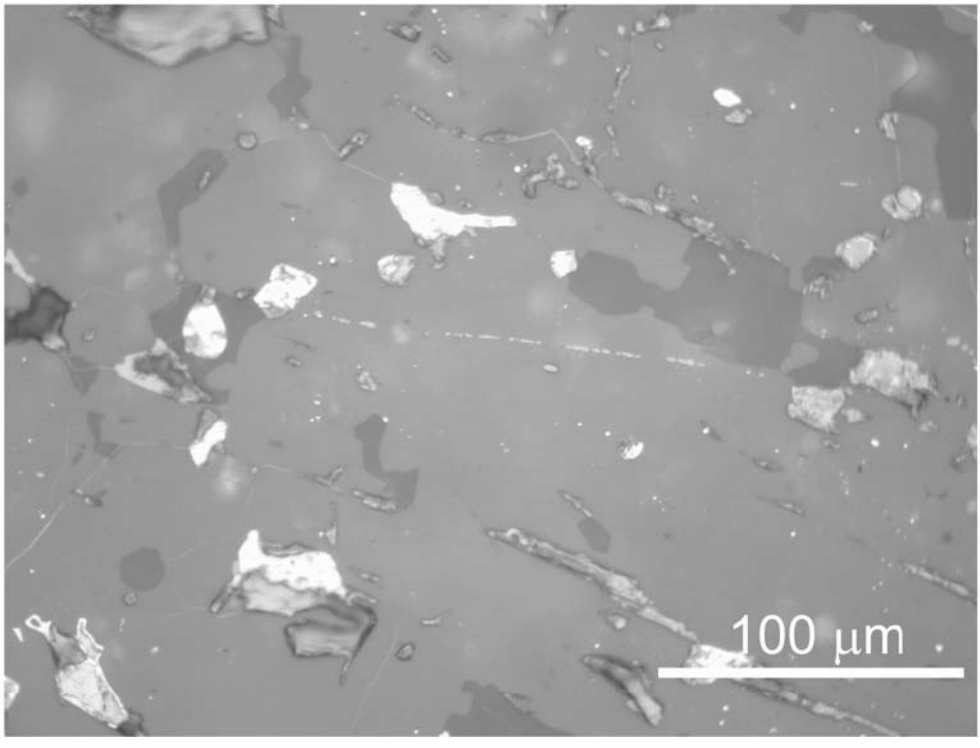

Fig. 8. Narrow chromite veinlet (light gray; center) transecting mafic silicate grains (medium gray) and occurring adjacent to melted plagioclase (dark gray; right). Reflected light.

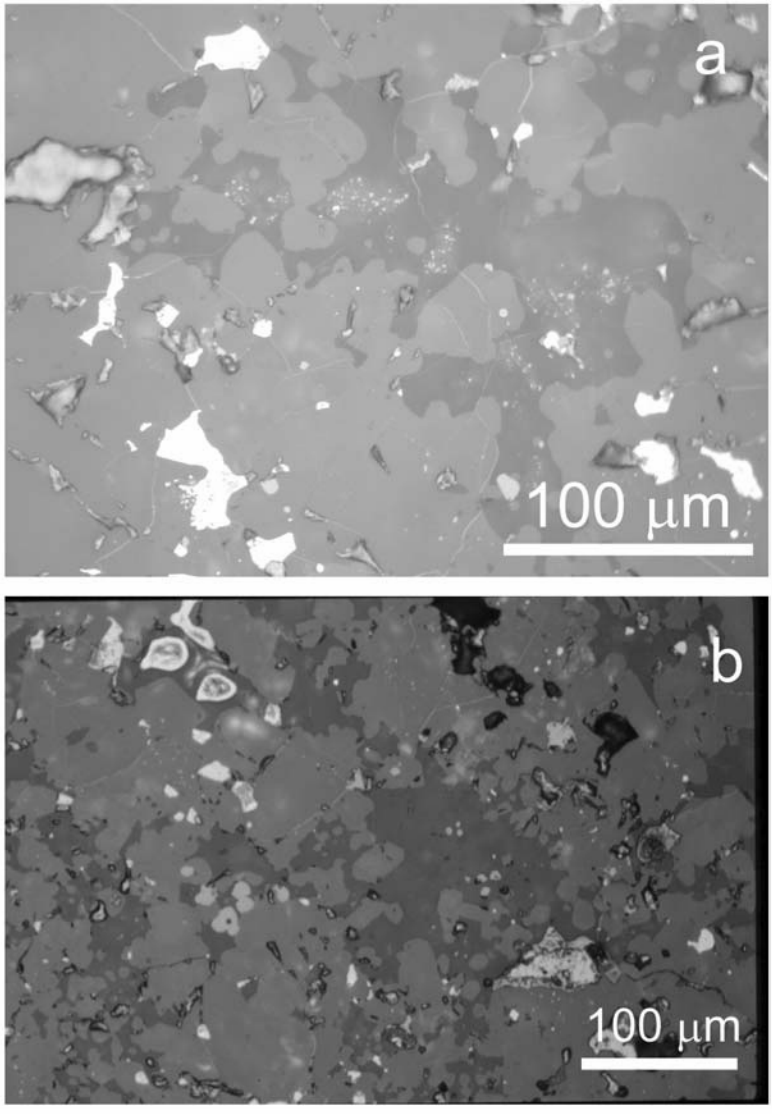

Fig. 9. Fine-grained chromite-plagioclase assemblages: a) melted, pincer-shaped plagioclase grain (dark gray) that contains several patches of very fine-grained chromite blebs (light gray). The assemblage has a high plagioclase/chromite modal abundance ratio; b) pincer-shaped plagioclase patches containing a few small chromite grains (center) and a few coarse chromite grains (left of center). Both images are in reflected light.

chromite (occurring as 0.1–5 μm-size euhedral, subhedral, rounded, and anhedral grains) and ~80 vol% plagioclase. Chromite grains are concentrated in the center of the assemblage; the outer 200 μm-thick region contains relatively few chromite grains. Approximately 0.5 vol% of the assemblage consists of small troilite blebs occurring among the small chromite grains. A few rounded 4 μm-diameter chromite grains are surrounded by 0.2 μm-thick troilite rims.

Several small chromite-plagioclase assemblages have textures that resemble one another. A typical example is the smallest (50 × 90 μm) assemblage, which contains 25 vol% chromite, present in the plane of the section as 4, relatively large (10–22 μm-size) grains and approximately a dozen small (0.3–2 μm-size) rounded blebs and angular grains.

The finest-grained assemblages consist of 95 vol% plagioclase and 5 vol% chromite occurring as 1–2 μm-size angular and rounded grains (Figs. 9a and 9b). As noted by Rubin (2003), a positive correlation seems to exist between chromite grain size and modal abundance in the chromite-plagioclase assemblages: finer-grained assemblages tend to contain smaller proportions of chromite.

DISCUSSION

Formation of Opaque Assemblages

Unshocked to weakly shocked type-4–6 OC contain opaque assemblages that consist of kamacite, taenite, and

troilite; no plessite (except zoneless plessite; see below) is present (e.g., Wood 1967). In contrast, abundant plessite occurs in those OC that have suffered appreciable degrees of shock. These rocks include L5 Kingfisher (Taylor and Heymann 1970), H5 Sweetwater (Taylor and Heymann 1971), H6 Guareña (Willis and Goldstein 1983), and LL6 MIL 99301 (Rubin 2002). Although zoneless plessite forms in chondrites during slow cooling (Sears and Axon 1975; Reisener and Goldstein Forthcoming), other forms of plessite are produced when highly localized stress concentrations resulting from an impact event heat kamacite-taenite intergrowths above the Fe-Ni solvus. Moderately rapid cooling could result in the formation of plessite. Alternatively, quenching could cause martensite formation, and martensite could unmix to form plessite during annealing. The fact that most metallic Fe-Ni grains in Spade contain plessite (Fig. 6) indicates that shock heating of the rock was pervasive.

Likely, during annealing, a large fraction of P diffused out of the metal and was oxidized to form Ca phosphate (Murrell and Burnett 1983) at the metal-silicate interface. Calcium was probably derived from plagioclase and pyroxene. Concomitant reduction of FeO to metallic Fe could have supplied the oxygen. If this is the case, then some of the small metal blebs within mafic silicate grains in Spade possibly formed by reduction of FeO and not by shock mobilization of metallic Fe-Ni.

Implications of Silicate Mineralogy

Plagioclase

Equilibrated OC tend to contain plagioclase that is relatively uniform in composition, e.g., Kernouvé (H6) plagioclase has a mean composition of $An_{11.4 \pm 0.8}$ and a range of 9.3 to 12.7 An (n = 12); Ogi (H6) plagioclase has a mean composition of $An_{12.5 \pm 0.4}$ and a range of 12.1 to 12.9 An (n = 7) (Rubin 1992). In contrast, Spade plagioclase has a moderately large range in composition ($An_{4.6–28.8}$; n = 24), that more closely resembles the ranges observed in the Rose City H chondrite impact-melt breccia ($An_{8.5–23.9}$; n = 11) and the moderately shocked (shock stage S4) Paragould LL5 chondrite ($An_{8.7–44.5}$; n = 16) (Rubin 1992).

Shock remelting may account for the compositional zoning of individual plagioclase grains in Spade. These grains have cores with relatively high CaO and low K_2O ($Ab_{68–71}Or_{2.2–2.5}$) and rims with relatively high Na_2O and K_2O ($Ab_{83–85}Or_{6–8}$), consistent with an igneous zoning pattern. Coarse plagioclase grains in equilibrated OC tend to have uniform (i.e., unzoned) CaO contents; they also tend to have nonuniform K_2O contents that vary by a factor of ~2 within individual grains (Van Schmus and Ribbe 1968). (However, the K_2O variations in plagioclase from equilibrated OC do not correlate with crystal geometry, i.e., no evidence exists for systematic compositional zoning of K_2O in these plagioclase grains.)

An impact melting history for plagioclase in Spade is consistent with the irregular, pincer shapes of the grains (Fig. 4). The grains appear to have melted and flowed; during this process, they partially to completely wrapped themselves around adjacent grains of mafic silicate. We have observed similar pincer-shaped plagioclase patches in the very strongly shocked (shock stage S6; Bennett and McSween 1996a) Kingfisher L5 chondrite.

Low-Ca Pyroxene

The CaO content of low-Ca pyroxene in Spade (3.5 ± 0.4 mol% Wo) exceeds that of unshocked H chondrites. The Wo content of low-Ca pyroxene grains in OC does not vary significantly among the H, L, and LL groups but does correlate weakly with petrologic type (Scott et al. 1986; Brearley and Jones 1998). Nevertheless, the Wo contents of low-Ca pyroxene in H4–6 chondrites do not generally exceed 2 mol%. Although the ALH A81187 acapulcoite has a relatively high Wo content ($Fs_{6.9}Wo_{3.2}$; Table 20 in Mittlefehldt et al. 1998), its Fs content is much lower than that of Spade (i.e., $Fs_{16.0 \pm 0.1}$), and it is not directly comparable.

Elevated Wo contents (~3 mol%) in low-Ca pyroxene were observed in material that equilibrated with partially molten chondritic material at 1200°C within a few days (Feldstein et al. 2001). In general, the CaO contents in low-Ca pyroxene correlate positively with the temperature of formation of the grains (whether these grains formed by crystallization from a melt, equilibration with a melt at high temperatures, or crystallization during thermal metamorphism) (e.g., Atlas 1952; Schairer and Boyd 1957; Dobretsov 1968).

Pyroxene thermometry can yield approximate equilibration temperatures for Spade. Because the Mg-Fe thermometer of Kretz (1982) gives temperatures that are too high for some pyroxene grains that were equilibrated experimentally (Lindsley 1983), the Lindsley thermometer is used here to estimate equilibration temperature. The Wo and Fs mole fractions of Ca pyroxene (0.385 and 0.140) and low-Ca pyroxene (0.035 and 0.160) were determined from the data in Table 2 following the projection scheme of Lindsley (1983) and Lindsley and Andersen (1983). Plotting these data on the 1 atm diagram (Fig. 6 in Lindsley and Andersen 1983) yields equilibration temperatures of 1100°C for Ca pyroxene and 1200°C for low-Ca pyroxene. (The Mg-Fe thermometer of Kretz [1982] yielded a much higher equilibration temperature, i.e., 1330°C.) The inferred equilibration temperatures derived from the Lindsley method are the same as (or somewhat higher than) that of the OC solidus temperature (~1100°C; Jurewicz et al. 1995), consistent with Spade having been at least partly melted.

A high temperature origin is, thus, likely for Spade and for rocks that contain low-Ca pyroxene compositions close to those of Spade ($Fs_{16.0}Wo_{3.5}$); the latter include some orthopyroxene-bearing ureilites (e.g., Y-74130; $Fs_{17.8}Wo_{4.2}$;

Table 23 of Mittlefehldt et al. 1998) and silicate inclusions in the Watson IIE iron ($Fs_{17.3}Wo_{3.7}$; Olsen et al. 1994).

Relict Chondrules and Coarse Mafic Silicate Grains

The low modal abundance of relict chondrules in Spade (1.8 vol%) compared to average H6 chondrites (11.4 vol%) suggests that >80% of the chondrules in Spade were obliterated. This is a lower limit. If Spade had been a normal H3 chondrite with 65–75 vol% chondrules (e.g., Table 1 in Rubin 2000) before the impact event, then >95% of the chondrules would have been obliterated. Chondrule obliteration can be caused by brecciation, metamorphic recrystallization, and impact melting. In view of the other evidence for shock (e.g., silicate darkening, melted plagioclase, chromite veinlets, chromite-plagioclase assemblages) and the inferred equilibration temperatures for pyroxene that are at or above the OC solidus, impact melting is likely to be primarily responsible for chondrule obliteration in Spade.

Chondrule loss by impact melting has been inferred previously for the Portales Valley H chondrite (Rubin et al. 2001) and the Abee EH enstatite chondrite (Rubin and Scott 1997). In both of these meteorites, the relict chondrules served as nucleation sites for mafic silicates growing from the surrounding impact melt. The same is true for Spade. As described above, some relict chondrules appear to be overgrown by numerous 25 μm-size olivine grains.

Isolated 200 μm-size mafic silicate grains in OC are probably derived from broken chondrules (e.g., Nelson and Rubin 2002). Spade contains far fewer of these grains (1.8 vol%) than average H5 and H6 chondrites (9.0 ± 2.1 vol% and 9.8 ± 2.1 vol%, respectively; Table 2 in Rubin et al. 2001). The low abundance of coarse mafic silicate grains in Spade most likely indicates that impact-melting destroyed ≥80% of the pre-existing coarse grains.

Chromite-Plagioclase Assemblages

Chromite-plagioclase assemblages occur in nearly every shock stage S3–S6 OC and are a useful petrographic indicator of shock (Rubin 2003, Forthcoming). Plagioclase has a low impedance to shock compression; that heat from shock-melted plagioclase caused adjacent chromite grains to melt seems plausible. Chromite crystallized from this melt. The residual melt quenched and chromite-plagioclase assemblages were produced.

Silicate Darkening and Chromite Veinlets

Silicate darkening is caused by the dispersion of small blebs of metal and/or troilite inside and around mafic silicate grains (Rubin 1992). This phenomenon results mainly from impact heating of metallic Fe-Ni and troilite grains above the eutectic temperature of 988°C and mobilization of the engendered melt.

The curvilinear trails of monomineralic chromite formed from chromite-plagioclase melts that were injected into fractures in adjacent silicate grains (Rubin 2003); the chromite crystallized and the residual plagioclase-rich melt continued to flow, eventually pooling to form irregularly shaped plagioclase patches and melt pockets. The extensive silicate darkening in Spade (among both coarse and fine mafic silicate grains) indicates that essentially all of the silicate grains in the whole-rock were invaded by metal-sulfide melts. Those silicate grains that did not melt retained the opaque melt trails; they, thus, appear dark when viewed microscopically in transmitted light.

Petrogenesis

We conclude that Spade is an impact-melt breccia that has undergone appreciable melting of its chondritic precursor material. Because melting was extensive, the petrologic type of Spade before the impact event is unclear. However, the low Al_2O_3 content of the matrix chromite grains (3.5 ± 0.7 wt%) compared to average H4–6 chondrites (5.6–7.3 wt% Al_2O_3; Bunch et al. 1967) may indicate that Spade's progenitor was H3; chromite with low Al_2O_3 occurs in some type-3 OC such as H3.6 Prairie Dog Creek (2.7 wt% Al_2O_3) and H/L3.9 Bremervörde (0.2 wt% Al_2O_3) (Bunch et al. 1967). Although, conceivably, Spade was metamorphosed and partly melted by the decay of ^{26}Al, the occurrence of chromite-plagioclase assemblages and chromite veinlets suggests that impact-melting was responsible for Spade's temperature excursion.

The shock event caused Spade to reach shock stage S6. Relict silicate grains became infused with metal-sulfide and chromite-rich melts, resulting in extensive silicate darkening and the production of chromite veinlets. Chromite-plagioclase assemblages also formed during the shock event. Plagioclase was melted and it flowed around nearby mafic silicate grains, partly enclosing some of them, resulting in the characteristic pincer shape of Spade plagioclase grains. Low-Ca pyroxene crystallizing from the melt (or equilibrating with the melt at high temperatures) acquired relatively high amounts of CaO. Metallic Fe-Ni cooled rapidly below the Fe-Ni solvus and transformed into martensite. Subsequent reheating of the rock (discussed below) may have been responsible for the unmixing of the martensite and the development of plessite. Coarse grains of phosphate associated with the metallic Fe-Ni probably also grew during post-shock annealing.

Burial and Exhumation

There are ambiguities in the shock stage assignment of Spade. High shock stages (S3–S6) are indicated by the extensive silicate darkening (Rubin 1992) and the occurrence of chromite-plagioclase assemblages and chromite veinlets

(Rubin 2002, 2003). The impact-melted characteristics of Spade indicate shock stage S6 (corresponding to 45–60 GPa; Stöffler et al. 1991; Schmitt et al. 1994; Schmitt and Stöffler 1995). If the rock had been shocked to S6 levels and left otherwise undisturbed, the olivine grains would have exhibited planar fractures, planar deformation features and pronounced mosaic extinction (Stöffler et al. 1991). Also, likely, low-Ca clinopyroxene would have formed: Hornemann and Müller (1971) and Stöffler et al. (1991) found that clinopyroxene lamellae parallel to (100) form within orthopyroxene grains at shock pressures as low as ~5 GPa.

However, olivine in Spade is characteristic of shock stage S2; it exhibits undulose extinction and lacks planar fractures and planar deformation features. In addition, low-Ca clinopyroxene appears to be absent. These features suggest that Spade may have been shocked to stage S6 and then annealed. Annealing temperatures must have exceeded 630°C (the temperature at which low-Ca clinopyroxene transforms into orthopyroxene; Boyd and England 1965; Grover 1972). The annealing temperatures experienced by normal type-5 and -6 OC (700–750°C and 820–930°C, respectively; Dodd 1981; Olsen and Bunch 1984) are below that inferred for Spade from pyroxene thermometry (1100–1200°C).

The absence of schreibersite associated with metallic Fe-Ni in Spade suggests that cooling was slow enough for P to have been oxidized and reacquired by phosphate.

Although shock-induced features in olivine seem to have been annealed, Spade retains heterogeneous feldspar compositions. These observations allow us to place constraints on the thermal history of the rock. Bauer (1979) showed that it is possible to anneal shock-induced microfractures in olivine in short times (20 minutes) in the temperature range 700–900ºC. However, longer heating times tend to produce recrystallized grains. The Na, K interdiffusion rates in alkali feldspar are on the order of 10^{-18} to 10^{-19} m^2 s^{-1} at about 800ºC (Hokanson and Yund 1986). This means that Na, K interdiffusion on a scale of several μm, sufficient to result in homogenization of the feldspar, would take place in about 1 yr.

These 2 indicators suggest that post-shock heating times were fairly short. This is consistent with the annealing period expected for rocks in close proximity to an impact crater, perhaps in a melted region beneath the crater floor or near hot debris within ejecta blankets at the asteroid surface. Global heating caused by the decay of ^{26}Al should occur over significantly longer time scales, i.e., millions of years (e.g., Bennett and McSween 1996b; Keil 2000).

Whole-rock annealing is also probably responsible for the unmixing of the martensite and the formation of plessite (Fig. 6). Cobalt and Fe partitioned into kamacite, and Ni partitioned into taenite.

Annealing seems unlikely to have been sufficiently precise to remove planar fractures and planar deformation features in olivine, obliterate mosaicism, and leave the olivine grains with undulose extinction. More probably, heating would have annealed Spade to S1 levels. During such an annealing episode, the olivine crystal lattices would have healed; strain would have been reduced, and the olivine grains would have developed sharp optical extinction.

If we assume that Spade was annealed to S1 levels, then the occurrence of undulose extinction in its olivine grains indicates that the rock was (very weakly) shocked again after annealing. This may have occurred during exhumation from the crater or from the ejecta blanket, possibly by the same collisional event that launched Spade off the H chondrite parent asteroid. This scenario identifies Spade as an H chondrite that experienced impact melting, post-shock annealing, and post-annealing shock.

Because Spade is an impact-melt breccia, no doubt exists that it was once severely shocked, most likely to shock stage S6. The lack of mosaic extinction of its relict olivine (i.e., grains that did not crystallize from the impact melt) indicates that Spade was annealed, thus, firmly establishing the case for post-shock annealing. Likely, significant amounts of material on OC asteroids experienced successive episodes of thermal metamorphism, shock metamorphism, and post-shock annealing. Some of this material may have been shocked again. Possibly, some OC material experienced multiple episodes of shock and annealing. This inference is consistent with the shock history inferred from ^{40}Ar-^{39}Ar studies of some impact-melt-bearing OC (Kunz et al. 1997).

Acknowledgments–We thank J. T. Wasson (UCLA) for discussions and Mr. J. Talbert and Dr. C. Barnes (Texas Tech University) for providing the sample of Spade. We appreciate the detailed and helpful reviews by E. R. D. Scott and A. Yamaguchi and the comments of Associate Editor H. Nagahara. This work was supported in part by NASA Grant NAG5–4766 (A. E. Rubin) and NASA Grant NAG5–9463 (R. H. Jones; J. J. Papike, P. I.).

Editorial Handling—Dr. Hiroko Nagahara

REFERENCES

Atlas L. 1952. The polymorphism of $MgSiO_3$ and solid state equilibria in the system $MgSiO_3$-$CaMgSi_2O_6$. *Journal of Geology* 60:125–147.

Bauer J. F. 1979. Experimental shock metamorphism of mono- and polycrystalline olivine: A comparative study. Proceedings, 10th Lunar and Planetary Science Conference. pp. 2573–2596.

Bennett M. E. and McSween H. Y. 1996a. Shock features in iron-nickel metal and troilite of L-group ordinary chondrites. *Meteoritics & Planetary Science* 31:255–264.

Bennett M. E. and McSween H. Y. 1996b. Revised model calculations for the thermal histories of ordinary chondrite parent bodies. *Meteoritics & Planetary Science* 31:783–792.

Bogard D. D., Garrison D. H., Norman M., Scott E. R. D. and Keil K. 1995. ^{39}Ar-^{40}Ar age and petrology of Chico: Large-scale

impact melting on the L chondrite parent body. *Geochimica et Cosmochimica Acta* 59:1383–1400.

Boyd F. R. and England J. L. 1965. The rhombic enstatite-clinoenstatite inversion. In *Annual report of the Director, Geophysical laboratory.* Washington D.C.: Carnegie Institution of Washington. pp. 117–120.

Brearley A. J. and Jones R. H. 1998. Chondritic meteorites. In *Planetary materials,* edited by Papike J. J. Washington D.C.: Mineralogical Soecity of Amercia. pp. 3-1–3-398.

Dobretsov N. L. 1968. Paragenetic types and compositions of metamorphic pyroxenes. *Journal of Petrology* 9:358–377.

Dodd R. T. 1981. *Meteorites—A petrologic-chemical synthesis.* New York: Cambridge University Press. 368 p.

Feldstein S. N., Jones R. H. and Papike J. J. 2001. Partial melting experiments on the Leedey L6 chondrite: The textural controls of melting. *Meteoritics & Planetary Science* 36:1421–1441.

Fodor R. V. and Keil K. 1976. Carbonaceous and non-carbonaceous lithic fragments in the Plainview, Texas chondrite: Origin and history. *Geochimica et Cosmochimica Acta* 40:177–189.

Grover J. E. 1972. The stability of low-clinoenstatite in the system $Mg_2Si_2O_6$-$CaMgSi_2O_6$ (abstract). *Transactions of the American Geophysical Union* 53:539.

Hokanson S. A. and Yund R. A. 1986. Comparison of alkali interdiffusion rates for cryptoperthites. *American Mineralogist* 71:1409–1414.

Hornemann U. and Müller W. F. 1971. Shock-induced deformation twins in clinopyroxene. *Neues Jahrbuch fuer Mineralogie* 6: 247–256.

Jarosewich E. 1990. Chemical analyses of meteorites: A compilation of stony and iron meteorite analyses. *Meteoritics* 25:323–337.

Jurewicz A. J. G., Mittlefehldt D. W., and Jones J. H. 1995. Experimental partial melting of the St. Severin (LL) and Lost City (H) chondrites. *Geochimica et Cosmochimica Acta* 59:391–408.

Keil K. 2000. Thermal alteration of asteroids: Evidence from meteorites. *Planetary and Space Science* 48:887–903.

Kretz R. 1982. Transfer and exchange equilibria in a portion of the pyroxene quadrilateral as deduced from natural and experimental data. *Geochimica et Cosmochimica Acta* 46:411–421.

Kring D. A., Swindle T. D., Britt D. T., and Grier J. A. 1996. Cat Mountain: A meteoritic sample of an impact-melted asteroid regolith. *Journal of Geophysical Research* 101:29353–29371.

Kunz J., Falter M., and Jessberger E. K. 1997. Shocked meteorites: Argon-40-argon-39 evidence for multiple impacts. *Meteoritics & Planetary Science* 32:647–670.

Lindsley D. H. 1983. Pyroxene thermometry. *American Mineralogist* 68:477–493.

Lindsley D. H. and Andersen D. J. 1983. A two-pyroxene thermometer. Proceedings, 13th Lunar and Planetary Science Conference. pp. A887–A906.

Mason B. and Wiik H. B. 1966. The composition of the Bath, Frankfort, Kakangari, Rose City, and Tadjera meteorites. *American Museum Novitates* 2272:1–24.

Mittlefehldt D. W. and Lindstrom M. M. 2001. Petrology and geochemistry of Patuxent Range 91501, a clast-poor impact melt from the L chondrite parent body and Lewis Cliff 88663, an L7 chondrite. *Meteoritics & Planetary Science* 36:439–457.

Mittlefehldt D. W., McCoy T. J., Goodrich C. A., and Kracher A. 1998. Non-chondritic meteorites from asteroidal bodies. In *Planetary materials,* edited by Papike J. J. Washington D.C.: Mineralogical Society of America. pp. 4:1–4:195.

Murrell M. T. and Burnett D. S. 1983. The behavior of actinides, phosphorus, and rare earth elements during chondrite metamorphism. *Geochimica et Cosmochimica Acta* 47:1999–2014.

Nelson V. E. and Rubin A. E. 2002. Size-frequency distributions of chondrules and chondrule fragments in LL3 chondrites: Implications for parent-body fragmentation of chondrules. *Meteoritics & Planetary Science* 37:1361–1376.

Olsen E. J. and Bunch T. E. 1984. Equilibration temperatures of the ordinary chondrites: A new evaluation. *Geochimica et Cosmochimica Acta* 48:1363–1365.

Olsen E. J., Davis A., Clarke R. S., Schultz L., Weber H., Clayton R. N., Mayeda T., Jarosewich E., Sylvester P., Grossman L., Wang M. S., Lipschutz M. E., Steele I. M., and Schwade J. 1994. Watson: A new link in the IIE iron chain. *Meteoritics* 29:200–213.

Reisener R. J. and Goldstein J. I. Forthcoming. The formation of zoned and unzoned metal particles in low-shock types 4–6 ordinary chondrites. *Meteoritics & Planetary Science*.

Rubin A. E. 1990. Kamacite and olivine in ordinary chondrites: Intergroup and intragroup relationships. *Geochimica et Cosmochimica Acta* 54:1217–1232.

Rubin A. E. 1992. A shock-metamorphic model for silicate darkening and compositionally variable plagioclase in CK and ordinary chondrites. *Geochimica et Cosmochimica Acta* 56:1705–1714.

Rubin A. E. 2000. Petrologic, geochemical, and experimental constraints on models of chondrule formation. *Earth-Science Reviews* 50:3–27.

Rubin A. E. 2002. Post-shock annealing of Miller Range 99301: Implications for impact heating of ordinary chondrites. *Geochimica et Cosmochimica Acta* 66:3327–3337.

Rubin A. E. 2003. Chromite-plagioclase assemblages as a new shock indicator; Implications for the shock and thermal histories of ordinary chondrites. *Geochimica et Cosmochimica Acta* 67: 2695–2709.

Rubin A. E. Forthcoming. Postshock annealing and postannealing shock in equilibrated ordinary chondrites: Implications for the thermal and shock histories of chondritic asteroids. *Geochimica et Cosmochimica Acta*.

Rubin A. E. and Scott E. R. D. 1997. Abee and related EH chondrite impact-melt breccias. *Geochimica et Cosmochimica Acta* 61: 425–435.

Rubin A. E., Rehfeldt A., Peterson E., Keil K., and Jarosewich E. 1983. Fragmental breccias and the collisional evolution of ordinary chondrite parent bodies. *Meteoritics* 18:179–196.

Rubin A. E., Ulff-Møller F., Wasson J. T., and Carlson W. D. 2001. The Portales Valley meteorite breccia: Evidence for impact-induced melting and metamorphism of an ordinary chondrite. *Geochimica et Cosmochimica Acta* 65:323–342.

Ruzicka A., Snyder G. A., Prinz M., and Taylor L. A. 1999. Portales Valley: A new metal-phosphate-rich meteorite with affinities to Netschaëvo and H-group chondrites (abstract #1645). 30th Lunar and Planetary Science Conference.

Schairer J. F. and Boyd F. R. 1957. Pyroxenes, the join $MgSiO_3$-$CaMgSi_2O_6$. *Annual report of the Director, Geophysical laboratory.* Washington D.C.: Carnegie Institution of Washington. pp. 223.

Schmitt R. T., Deutsch A. and Stöffler D. 1994. Shock recovery experiments with the H6 chondrite Kernouvé at preshock temperatures of 293 and 920 K (abstract). *Meteoritics* 29:529–530.

Schmitt R. T. and Stöffler D. 1995. Classification of chondrites (abstract). *Meteoritics* 30:574–575.

Scott E. R. D. 1982. Origin of rapidly solidified metal-troilite grains in chondrites and iron meteorites. *Geochimica et Cosmochimica Acta* 46:813–823.

Scott E. R. D., Taylor G. J., and Keil K. 1986. Accretion, metamorphism, and brecciation of ordinary chondrites: Evidence from petrologic studies of meteorites from Roosevelt County,

New Mexico. Proceedings, 17th Lunar and Planetary Science Conference. pp. E115–E123.
Sears D. W. and Axon H. J. 1975. The metal content of common chondrites (abstract). *Meteoritics* 10:486–487.
Stöffler D., Keil K., and Scott E. R. D. 1991. Shock metamorphism of ordinary chondrites. *Geochimica et Cosmochimica Acta* 55: 3845–3867.
Takeda H., Huston T. J., and Lipschutz M. E. 1984. On the chondrite-achondrite transition: Mineralogy and chemistry of Yamato-74160 (LL7). *Earth and Planetary Science Letters* 71: 329–339.
Taylor G. J. and Heymann D. 1970. Electron microprobe study of metal particles in the Kingfisher meteorite. *Geochimica et Cosmochimica Acta* 34:677–687.
Taylor G. J. and Heymann D. 1971. Postshock thermal histories of reheated chondrites. *Journal of Geophysical Research* 76:1879–1893.
Van Schmus W. R. and Ribbe P. H. 1968. The composition and structural state of feldspar from chondritic meteorites. *Geochimica et Cosmochimica Acta* 32:1327–1342.
Wilkening L. L. 1978. Tysnes Island: An unusual clast composed of solidified, immiscible, Fe-FeS and silicate melt. *Meteoritics* 13: 1–9.
Willis J. and Goldstein J. I. 1983. A three dimension study of metal grains in equilibrated, ordinary chondrites. Proceedings, 14th Lunar and Planetary Science Conference. pp. B287–B292.
Wlotzka F. 1993. A weathering scale for the ordinary chondrites (abstract). *Meteoritics* 28:460.
Wood J. A. 1967. Chondrites: Their metallic minerals, thermal histories, and parent planets. *Icarus* 6:1–49.
Yamaguchi A., Scott E. R. D., and Keil K. 1998. Origin of unusual impact melt rocks, Yamato-790964 and -790143 (LL chondrites). *Antarctic Meteorite Research* 11:18–31.
Yamaguchi A., Scott E. R. D., and Keil K. 1999. Origin of a unique impact-melt rock—The L chondrite Ramsdorf. *Meteoritics & Planetary Science* 34:49–59.